JOURNAL OF COMPUTATIONAL PHYSICS 51, 261–272 (1983)

Numerical Evaluation of Magnetic Coordinates for Particle Transport Studies in Asymmetric Plasmas

GIOIETTA KUO-PETRAVIC AND ALLEN H. BOOZER

Plasma Physics Laboratory, Princeton University, Princeton, New Jersey 08544

AND

JAMES A. ROME AND RONALD H. FOWLER

Oak Ridge National Laboratory, P.O. Box Y, Oak Ridge, Tennessee 37830

Received December 8, 1981; revised January 26, 1983

A numerical procedure is described for the evaluation of magnetic coordinates given a toroidal, scalar pressure plasma with an arbitrary magnetic field. The accurate representation of magnetic field strength in this way is invaluable for the calculation of drift orbits and transport in asymmetric plasmas.

INTRODUCTION

Particle transport in thermonuclear plasmas depends basically on the number of directions of symmetry in the plasma configuration. The search for toroidal confinement devices alternative to the tokamak has led to systems like the stellarator, heliac, etc., all with less symmetry and consequently enhanced diffusion, especially at low collisionality regimes. Even for the tokamak, asymmetry effects are important for it is well known that a tokamak ripple of 1% or less is able to significantly enhance the ion loss. Therefore, any numerical technique enabling us to understand asymmetric plasmas would be most welcome. Deficiencies in our tools have long been recognized. Not only are the equilibrium and stability properties difficult to simulate, but even the single particle confinement characteristics are largely unknown. In these asymmetric configurations coordinates based on the magnetic field lines become the natural coordinates to use as it is intrinsically capable of higher accuracy and speed. In this system, the rapid motion of particles parallel to the field line is well-separated from the slow drift motion across the field lines, and hence large errors arising from numerical diffusion is avoided. It has been realized both computationally [1] and, more recently, experimentally [2] that the presence of an electric field is essential to good particle confinement in stellarators. Since electric potential is uniform over a flux surface, the magnetic coordiantes provide an extremely easy method of incorporating electric field effects. The usefulness of magnetic coordinates has long been

0021-9991/83 $3.00

recognized in plasma equilibrium and stability studies [3–5]. Recently it was shown [6–8] that the guiding center drift equations are particularly simple in magnetic coordinates requiring only a knowledge of the scalar quantity B, the magnetic field strength, and its derivatives. From this it follows that particle transport, with and without collisions, may be readily computed to a high degree of accuracy with a minimum of computer time and storage.

However, the correspondence between the magnetic coordinates and the Cartesian system remains a difficult problem. In this paper we describe the realization of a technique [9] whereby the magnetic field strength is computed in magnetic coordinates by Fourier decomposition for a toroidal plasma with scalar pressure equilibrium and closed magnetic surfaces. This procedure assumes a knowledge of the magnetic field $B(R, Z, \Phi)$ at all points in the torus, where R, Z, and Φ are the cylindrical coordinates. This field can be derived from a combination of external current filaments and plasma currents, assuming that the plasma equilibrium is known.

The Magnetic Coordinates and Their Derivation

The appropriate magnetic coordinates for transport studies have a simple covariant and contravariant representation for **B**. In a scalar pressure equilibrium

$$\nabla p = \frac{1}{c}\mathbf{j} \times \mathbf{B},$$

these coordinates [6] are ψ, θ_0, χ with

$$\begin{aligned} \mathbf{B} &= \nabla\psi \times \nabla\theta_0 \qquad \text{contravariant} \\ &= \nabla\chi + \beta\nabla\psi \qquad \text{covariant.} \end{aligned} \tag{1}$$

Here $2\pi\psi$ is the toroidal magnetic flux inside a magnetic surface, χ is the generalized magnetic potential $\chi = \int \mathbf{B} \cdot \mathbf{d}l$, and θ_0 is an angle which labels the field lines.

The usefulness of magnetic coordinates (ψ, θ_0, χ) can best be illustrated by deriving the simple guiding center drift equations in a general field **B** in these coordinates. The guiding center velocity **v** can be written [8, 10]

$$\mathbf{v} = \frac{v_\parallel}{B}\left[\mathbf{B} + \nabla \times \rho_\parallel \mathbf{B}\right],$$

where $\rho_\parallel$, the parallel Larmor radius, is

$$\rho_\parallel = \frac{v_\parallel}{(eB/mc)}. \tag{2}$$

The drift equations are

$$\begin{aligned}
\frac{d\psi}{dt} &= -c\frac{\partial V}{\partial \theta_0} - \left(\frac{c}{e}\mu + \frac{eB}{mc}\rho_{\|}^2\right)\frac{\partial B}{\partial \theta_0}, \\
\frac{d\theta_0}{dt} &= +c\frac{\partial V}{\partial \psi} + \left(\frac{c}{e}\mu + \frac{eB}{mc}\rho_{\|}^2\right)\frac{\partial B}{\partial \psi}, \\
\frac{d\chi}{dt} &= \frac{eB^2}{mc}\rho_{\|}^2, \\
\frac{\partial p_{\|}}{dt} &= -c\frac{\partial V}{\partial \chi} - \left(\frac{c}{e}\mu + \frac{eB}{mc}\rho_{\|}^2\right)\frac{\partial B}{\partial \chi},
\end{aligned} \tag{3}$$

where (eB/mc) is the ion cyclotron frequency, $\frac{1}{2}mv_{\perp}^2 = \mu B$, V is the electrostatic potential, and c is the velocity of light.

In a torus, poloidal, and toroidal angles, θ and ϕ, respectively, can be defined such that [7]

$$\chi = g(\psi)\phi + I(\psi)\theta, \tag{4}$$

$$\theta = \theta_0 + \iota(\psi)\phi, \tag{5}$$

where $(c/2)\,g(\psi)$ is the total poloidal current outside a flux surface ψ, $(c/2)\,I(\psi)$, the total toroidal current inside a flux surface ψ, and $\iota(\psi)$, the rotational transform.

The periodicities in θ and ϕ in a torus enable us to write down for any scalar function like B, the magnetic field strength [9]

$$B(\psi, \theta, \phi) = \sum_{n,m} \{a_{nm} \exp[i(n\phi - m\theta)]\}. \tag{6}$$

Using (4) and (5) we obtain

$$n\phi - m\theta = \frac{n - m\iota}{g + \iota I}\chi - \frac{mg + nI}{g + \iota I}\theta_0. \tag{7}$$

We assume that $B(R, Z, \Phi)$ in a cylindrical system is numerically known anywhere within the torus. We can integrate along a field time to obtain $B(\chi)$, where χ is the magnetic coordinate along the field line derived from (2) as

$$\chi = \int B\, dl,$$

where dl is a differential distance along the field line.

Since a field line must obey $\psi = \text{constant}$ and $\theta_0 = \text{constant}$ by definition

throughout this integration, we can choose our initial point to be $(\psi, 0, 0)$ and obtain the simplified equation

$$B(\chi) = \sum_{n,m} |a_{nm} \exp(i\omega_{nm}\chi)|,$$

$$\omega_{nm} = \frac{n - m\iota}{g + \iota I}. \tag{8}$$

Since $B(\chi)$ is in general not a periodic function unless ψ happens to coincide with a rational surface, it is necessary to limit the extent of the integration in χ by the use of a window function, a concept widely used in combination with fast Fourier transforms (FFT) in electronics [11, 12]. The FFT assumes a periodic function as input, therefore the mismatch in $B(\chi)$ at the ends of integration $\chi = \pm\chi_*$ will give rise to spurious noise in the Fourier spectrum which can be minimized by the appropriate choice of the window function. We shall in this paper use a Gaussian window as it is analytic, hence easily understood. This Gaussian should have a width much smaller than the range of integration χ_*, but broader compared to the frequencies of interest in $B(\chi)$. Let $A(\omega)$ be the Fourier transform of $B(\chi)$ times a Gaussian of width χ_*/η:

$$A(\omega) \equiv \int_{-\chi_*}^{\chi_*} B(\chi) \left[\frac{\eta}{(2\pi)^{1/2}\chi_*} \exp\left(-\frac{\eta^2}{2}\frac{\chi^2}{\chi_*^2}\right) \right] \exp(-i\omega\chi)\, d\chi$$

$$= \int_{-\chi_*}^{\chi_*} F(\chi) \exp(-i\omega\chi)\, d\chi, \tag{9}$$

then

$$A(\omega) = \sum_{n,m} a_{nm} \exp\{-\tfrac{1}{2}|(\omega_{nm} - \omega)/\omega_*|^2\},$$

where $\omega_* = \eta/\chi_*$ gives the broadening of the spectrum to be expected from a Gaussian of width χ_*/η. By adjusting the parameter η, the width of the Gaussian may be tuned to give minimum mismatch at $\chi = \pm\chi_*$ consistent with a clear separation in the Gaussian maxima of the function $A(\omega)$.

The values of a_{nm} and ω_{nm}, extracted from the Fourier spectrum, can be used in Eq. (8) to produce $B(\psi, \theta_0, \chi)$.

Application to a Torsatron

Figure 1 shows the coil configuration of a $l = 2$ $M = 10$ torsatron with major radius of 1.7 meters and minor radius of 0.4 meters.

Since the point $\chi = 0$ is arbitrary, it is convenient to choose a point of symmetry in χ as this reference point, for when the input is symmetric, the output Fourier spectrum will lie entirely in the real frequency plane. Therefore we start the integration at point $B(\psi, 0, 0)$ in one of the symmetry planes of the torus. The value

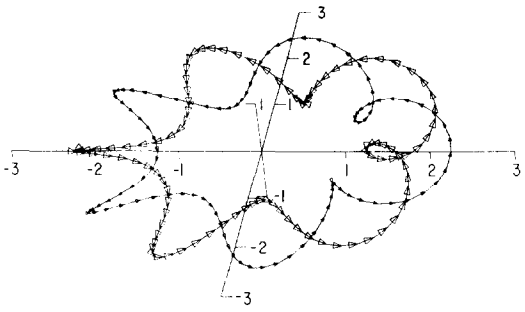

FIG. 1. 3-D view of the coil configuration of a $l = 2$ $m = 10$ torsatron.

of ψ will not be known until after the integration is completed and many toroidal circuits have been traced. We solve the equations for the field line in χ, thus ensuring that we have B in equal intervals of χ:

$$\frac{dR}{d\chi} = \frac{B_R}{B^2},$$

$$\frac{dZ}{d\chi} = \frac{B_Z}{B^2},$$

$$\frac{d\Phi}{d\chi} = \frac{B_\Phi}{RB^2}. \tag{10}$$

A fourth-order Runge–Kutta integration scheme or, alternatively, a modified divided

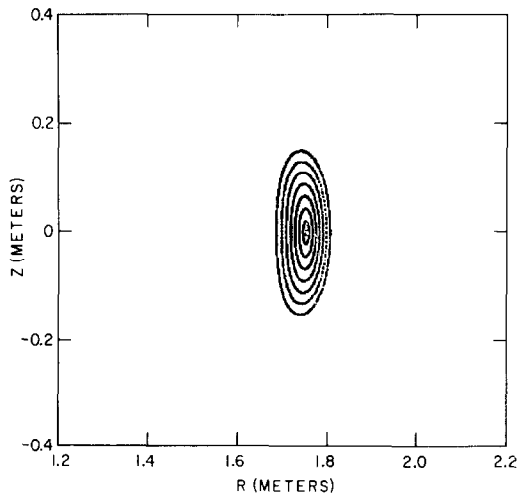

FIG. 2. The intersections of eight magnetic surfaces with a symmetry plane.

difference method of Shampine and Gordon [13] has been used, and at each step we save both the value of B as well as the associated R, Z, Φ. Figure 2 shows the intersections of eight field lines with a symmetry plane, each tracing out a separate flux surface. To obtain a precise value of ψ, two methods have been used: (1) Since B_ϕ is given by the sum of poloidal currents, g, threading the torus, $B_\phi = g/R$ and

$$\psi = \frac{1}{2\pi} \int B_\phi \, dR \, dz = \frac{1}{2\pi} \int \frac{g}{R} \, dR \int dz. \tag{11}$$

(2) Area integration becomes progressively more complex when the shape of the area becomes more irregular. Under these circumstances we convert the area integral to a line integral in the vector potential A

$$\psi = \oint \mathbf{A} \cdot \mathbf{ds}.$$

The integration path which is mapped by a bi-cubic spline consists of the intersection of the flux surface with the symmetry plane. The vector potential in general is obtainable from the magnetic field package.

Our purpose is to obtain the amplitudes of the Fourier peaks and identify their mode numbers n and m. A judicious choice of the parameters χ_*, η, $\Delta\chi$, N, where $\Delta\chi$ is the step length of integration and N the total number of data points, will aide in much savings for both computer time and storage. Naturally $\Delta\chi$ should be chosen to satisfy certain accuracy criterion on $B(\chi)$. The total number of points N is in general limited by the available computer time and storage. As can be seen from Eq. (7) or Fig. 5 the smallest distance between consecutive peaks in the Fourier spectrum is approximately ι/g if $\iota < 1$ and $I \ll g$. Therefore in cases where the peak separation is large enough, a broad peak width, arising from Gaussian broadening, η/χ_*, may be tolarated. As is generally the case, we have conflicting requirements on η, the Gaussian width. On the one hand, η should be small to minimize the Fourier peak width, on the other hand, the width of the Gaussian, χ_*/η, should be kept small in order to minimize noise arising for the mismatch at $\chi = \pm\chi_*$. Let us assume that we allow Gaussian broadening on the Fourier peaks to be twice the intrinsic resolution of the peaks which is given by $2\pi/2\chi_*$; we have, therefore, $\omega_* = \eta/\chi_* = 2(\pi/\chi_*)$ and $\eta = 2\pi$. This then determines η. The maximum frequency in the output of a Fourier analyzer is, of course, dependent only on $\Delta\chi$, the minimum distance between input data points. However, if we were to keep $\Delta\chi$ the same but increase the range of the input to $-p\chi_* < \chi < p\chi_*$, where $p > 1$, a better resolution would be obtained in the sense that there would be p times more points per given output interval. A very simple way of achieving this without spending more time on the integration of $B(\chi)$ is simply to fill up the input beyond χ_* with zeros. If η is kept the same then the Gaussian broadening, ω_*, would also be reduced. Of course a certain amount of noise is introduced, but this should be small since the Gaussian envelope has already reduced the input at $p\chi_*$ to $e^{-2\eta}$ times the value at $\chi = 0$. The smallest frequency

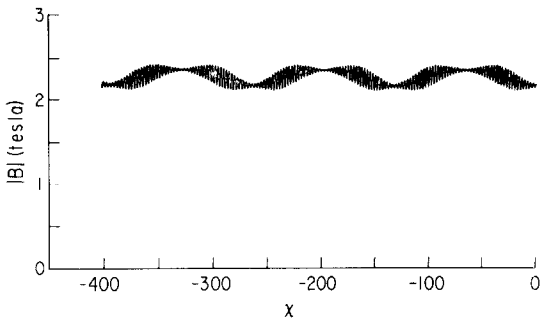

FIG. 3. Magnetic field $B(\chi)$ along a field line. $\chi = \int B\, dl$.

difference, $\Delta\omega$, which we wish to resolve is either ι/g or $1/g$, whichever is the smaller; suppose we require that this $\Delta\omega$ be a few times, say η times the line width, ω_*, then $\Delta\omega = \eta\omega_* = \eta^2/\chi_*$ and $\chi_* = \eta^2/\Delta\omega$. Taking $\Delta\omega = \iota/g$ and $\chi = g\phi$, it may be seen that we need to follow the field line at least η^2/ι toroidal circuits in order to have distinct peak separation. One last choice available to us lies in $\chi_* = N\,\Delta\chi$. Since we are often interested in only the very low frequency end of the Fourier spectrum, it is useful to minimize N and correspondingly increase $\Delta\chi$ so as to save integration time. However, $\Delta\chi$ must be kept sufficiently small to accurately follow the field lines.

Figure 3 shows a plot of $B(\chi)$ versus χ for 2^{13} points in the range $-\chi_* < \chi < 0$. The other half may be obtained by reflection because of the inherent up down symmetry of the coil configuration. This $B(\chi)$ is then multiplied with a Gaussian with $\eta = 4$ to provide the input to a fast Fourier transform package. Figure 4 shows a section of the Fourier spectrum. Since in most cases the currents are predominently poloidal, that is, $I \ll g$, it is convenient to plot a_{mn} against $(n - m\iota)$ rather than ω_{nm}, for peaks with $m = 0$ appear then as integers on the absissa. The separations between peaks with common n also give us a good method of estimating the average transform ι. Values

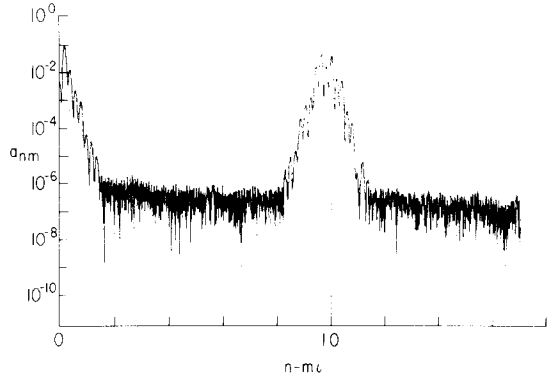

FIG. 4. Fourier spectrum at one flux surface showing the real coefficients a_{nm} versus $(n - m\iota)$ for a torsatron.

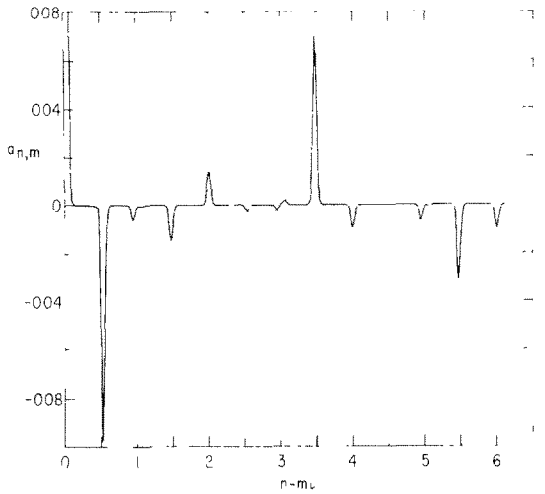

FIG. 5. Fourier spectrum at one flux surface showing the real coefficients a_{nm} versus $(n - mι)$ for a heliac.

of these coefficients can be obtained by these means to within an order of accuracy of $\sim 10^{-3}$. Appearance of the spectrum depends very much on the toroidal and poloidal mode numbers of the configuration as well as the transform and the poloidal and toroidal currents involved in producing the magnetic field. Another example of a spectrum can be seen in Fig. 5, where the $n = 2$, $m = 1$ configuration of a heliac Torsatron gives rise to a fewer number of more separated peaks.

Figure 6 is a 3-D plot of the amplitude of the Fourier peaks in n, m space. After

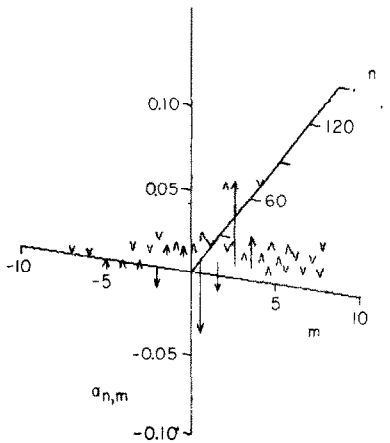

FIG. 6. 3-D display of Fourier coefficients a_{nm} in n, m space shown in Fig. 4.

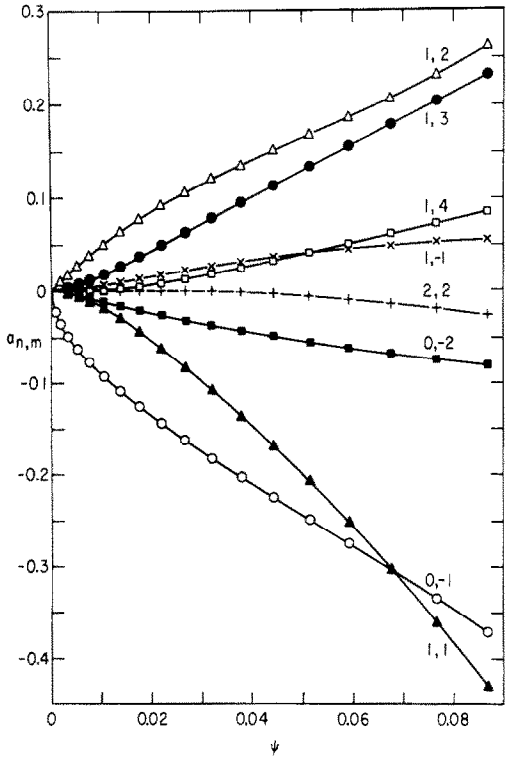

FIG. 7. Variations of some Fourier coefficients a_{nm} with toroidal flux ψ.

identifying a chosen number of the largest Fourier coefficients at several flux surfaces, we now have the complete information for reconstruction,

$$B = \sum_{n,m} a(\psi) \cos\left(\frac{n - m\iota}{g + \iota I}\chi - \frac{mg + nI}{g + \iota I}\theta_0\right), \tag{12}$$

if we assume that variations of $a_{n,m}$ with ψ may be obtained by spline or polynomial interpolation. Figure 7 shows all the coefficients used with cubic spline fits. Figure 8 shows the variation of the rotational transform ι with ψ, again using spline fits.

In order to check our numerical process, we have compared the guiding center motion of a 10 KeV test particle using (1) magnetic field B, derived from current filaments by Biot–Savart law and standard drift equations in cylindrical coordinates and (2) magnetic field B in magnetic coordinates as described in this paper and the corresponding equations of motion Eq. (3). Figure 9a shows the magnetic field B, from the Biot–Savart law along the trajectory of the particle, and Fig. 9b shows the error in B along the trajectory where e_B is defined as

$$e_B = \frac{B_1 - B_2}{B_1 + B_2},$$

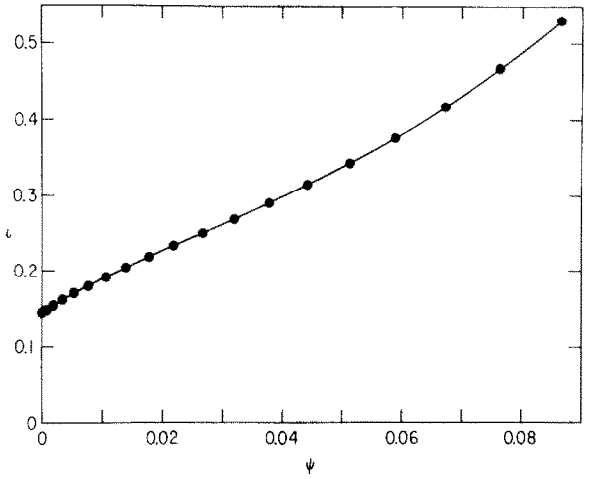

FIG. 8. Variation of the rotational transform ι with toroidal flux ψ.

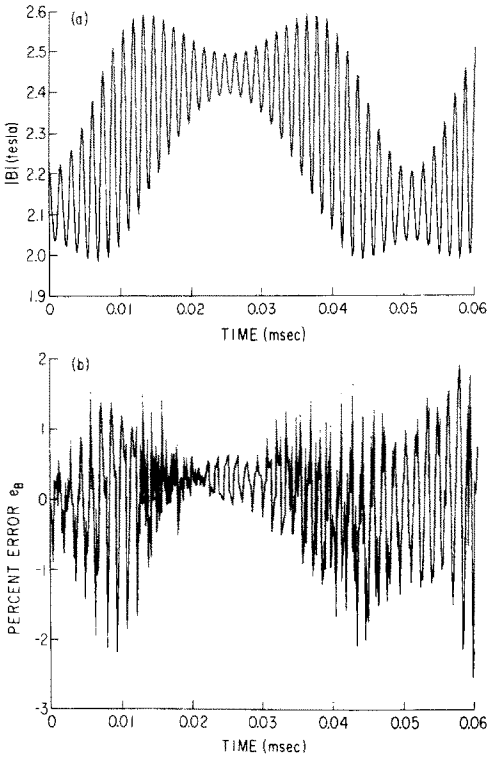

FIG. 9. (a) Magnetic field as calculated from the Biot–Savart law along the trajectory of the test particle with 10 KeV energy. (b) Percentage differences of magnetic field calculated in the cylindrical and magntic coordinate systems of the test particle along its trajectory.

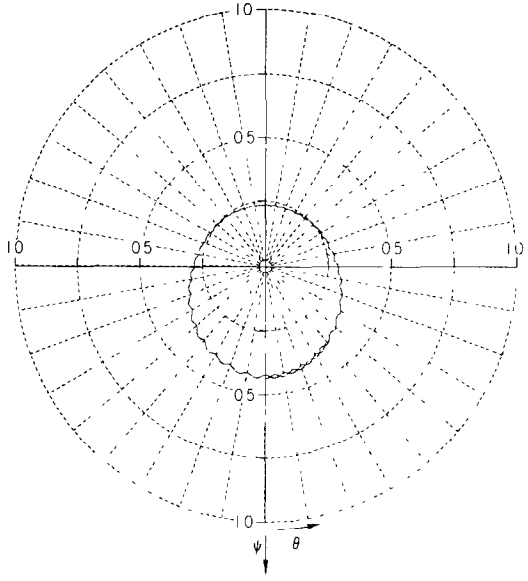

FIG. 10. Projection of the test particle of Fig. 9 onto the ψ, θ plane, where θ is the poloidal angle.

the subscripts 1 and 2 denote the two systems. This error can be regarded as a relative error of method (2) if one assumes that B_1 is the exact field. An order of magnitude gain in computer time was found for method (2). The errors in $v_{\|}$ and $v_{\perp}$ can also be measured in the same way and they give rise to variations similar to that shown in Fig. 9(b).

In Fig. 10 we show the trajectory of the test particle as a projection onto a given plane in polar coordinates where the angular coordinate is θ_0 and the radial coordinate $\psi \sim r^2$. It is easy to discern the deviation of a particle from a flux surface. In fact the adoption of the magnetic coordinates has made particle trajectories more physical and readily interpretable.

ACKNOWLEDGMENT

This work was supported by U.S. Department of Energy Contract No. DE-AC02-76-CHO-3073 and W7405-eng-26.

REFERENCES

1. G. KUO-PETRAVIC AND A. H. BOOZER, to be published.
2. G. GRIEGER, Wendelstein Results From IPP, Garching, Germany, private communication.
3. M. D. KRUSKAL AND R. M. KULSRUD, *Phys. Fluids* **1** (1958), 265.
4. S. HAMADA, *Nucl. Fusion* **2** (1962), 23.

5. J. M. GREENE AND J. L. JOHNSON, *Phys. Fluids* **5** (1962), 510.
6. A. H. BOOZER, *Phys. Fluids* **23** (1980), 904.
7. A. H. BOOZER, *Phys. Fluids* **24** (1981).
8. A. H. BOOZER AND G. KIU-PETRAVIC, *Phys. Fluids* **24** (1981), 851.
9. A. H. BOOZER, *Phys. Fluids* **25** (1982), 520.
10. P. H. RUTHERFORD, *Phys. Fluids* **13** (1979), 482.
11. F. J. HARRIS, *Proc. IEEE* **66** (1978), 51.
12. G. D. BERSLAND, *IEE Spectrum* **6** (1969), 41.
13. L. F. SHAMPINE AND M. K. GORDON, "Computer Solution of Ordinary Differential Equation," Freeman, San Francisco, 1975.